THE CHARACTERIZATION OF FOOT FORCE VECTOR CONTROL IN HUMAN STANDING

by

Kieran M. Nichols

A thesis submitted in partial fulfillment of
the requirements for the degree of
Master of Science
Kinesiology (Biomechanics)
at the
UNIVERSITY OF WISCONSIN-MADISON
2016

COMMITTEE MEMBERS

DR. KREG GRUBEN

DR. PETER VAN KAN

DR. PETER ADAMCZYK

TABLE OF CONTENTS

ABSTRACT

Interestingly, humans have the ability to produce many variations of foot force due to a multitude of joint torque combinations. The purpose of this thesis was to investigate if the neural system employs some particular coordination strategies and to evaluate how those variations relate to the mechanical requirements of standing. This thesis specifically explored variation in foot force to create Intersection Points (*IPs*) in unperturbed standing by analyzing how the mechanical variables of center of pressure, horizontal, and vertical forces covary. These mechanical variables were recorded on a calibrated custom force plate during unperturbed human standing, and frequency analyses were performed to quantify coordination. The data showed that humans tended to use a consistent coordination that caused a frequency dependent distribution of *IPs*. This distribution included lower frequency (0 -1.5 Hz) variation of the forces with high *IPs* (above the center of mass) and higher frequency (above 2 Hz) variation with low *IPs* (below the center of mass). The high *IPs*, which had most of the signals' power, slowly restore whole body angular orientation to upright, while not disrupting horizontal *CM* position. Whereas, the low *IPs* quickly restore translational position, but rotate the whole body angular position away from upright. The frequency dependent intersection point behavior demonstrates a simplified representation of how the neuromuscular coordination strategies control the force of the ground on the body to maintain upright standing balance.

TERMINOLOGY

Sagittal Plane

The vertical plane dividing the human body into left and right halves. All analyses were conducted in the sagittal plane. +z superior and +x anterior. (Figure 1)

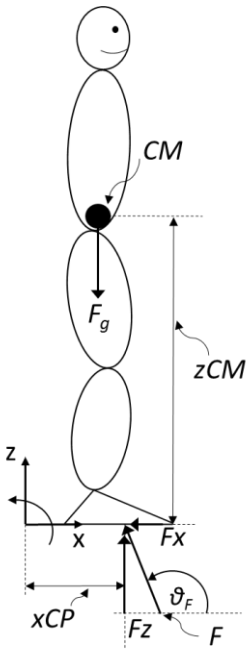

Figure 1: Reference frame and key variables

Ground on Feet Force (*F*)

The net force of the ground on the two feet (*Fx, Fz*). Commonly called the ground reaction force (GRF) in other literature.

Force Direction (θ_F)

The angle of the *F* vector with respect to the positive x-axis. Counterclockwise is positive for a right facing person

Center of Pressure (*xCP*)

The location of application of the vertical component of *F*.

Center of Mass (*xCM, zCM*)

The point that is the weighted average position of the mass of the body.

Whole Body Angular Position (*WBAP*)

The orientation (angle) that is the weighted average orientation of the segments of the body measured counterclockwise from the positive x-axis.

Force ratio (*Fr*)

The quotient of *Fx* and *Fz*

Intersection Point (*IP*)

The point at which a set of *F* lines of action intersect.

1. INTRODUCTION

1.1 Preface

This thesis aims to further the understanding of how humans maintain upright posture in unperturbed standing, as expressed in variation patterns in the force of the ground on the feet.

1.2 Mechanical Requirements of Standing

The force of the support surface on the human body is useful for characterizing standing as it represents the final common output of complex neuro-musculo-skeletal interactions and satisfies the mechanical constraints of physics necessary to maintain an upright posture. Unperturbed standing is the behavior of a human remaining in a posture similar to anatomical, where the only external forces acting on the body are due to gravity (*Fg*) and the ground on the feet (*F*). For the scope of this study, standing will be defined as the large segments (shank, thigh, torso) remaining within 30 degrees of vertical and having average translational and rotational velocity of zero (over a reasonably long but finite period of time). These conditions necessitate force of the ground on feet to have an average vertical component equal and opposite to the force of gravity. Two other aspects of that *F* requirement are that the average horizontal component (frictional force) and the average torque about the center of mass must also be zero. The ability to remain upright outside of these constraints is possible (Otten, E., 1999) but does not

constitute the typical unperturbed standing studied here. This mechanical description motivates the identification of which mechanical variables are of primary importance in analyzing human standing and how humans typically modulate those variables within the constraints due to physics.

To ensure unperturbed standing, the neural system utilizes the mechanical structures of bones, muscles, and tendons. These structures give the nervous system the ability to alter the force of the ground on the feet (*F*). In the sagittal plane, *F* can be described by its horizontal and vertical components (*Fx*, *Fz*) and location of the center of pressure (*xCP*). *F* and *Fg* determine the translational and rotational acceleration of the whole body. With appropriate analysis, these mechanical variables can provide insight into the nature of the neural control of standing posture.

1.3 Models of standing

In an attempt to represent the human with the simplest possible mechanical model, early researchers (Winter et. al 1998) proposed that ankle stiffness control of a single inverted pendulum (SIP) was suitable for controlling unperturbed standing.

The SIP consisted of a stick body and a massless foot. The stick had a distributed mass, and the ankle torque controlled the rotational motion of that mass about

the ankle joint. The forces acting on the body were the force from the floor (*F*) and gravity (*Fg*). The model derived that the horizontal distance from the center of pressure (*CP*) to the center of mass (*CM*) is proportional to the horizontal acceleration of the *CM*. This model also thereby demonstrates that the control of horizontal force is necessary to keep the SIP model upright due to the translational and rotational equations of its motion.

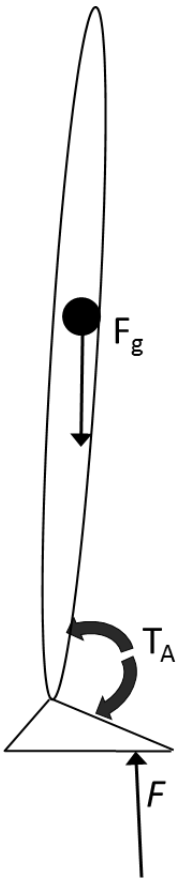

Figure 2 showing the SIP model with T_A being the ankle torque.

The SIP model assumed that ankle torque solely controlled the rotational motion of the body, and other joints (like the hip and knee) were controlled to keep these joints rigid. The control was simulated as a passive rotational spring, at the ankle, that has an effective stiffness sufficient to bring the body back to the upright position. To refute the sufficiency of balance control solely by ankle stiffness control, Loram and Lakie (2002) provided evidence that the intrinsic ankle stiffness observed in humans was not large enough (it was on average 91% of the necessary stiffness), to keep a passive mechanical model of the human upright.

To create a model that better represents human behavior, Gunther et. al (2011) showed that the Double Inverted Pendulum (DIP) better estimates the frequency content of the forces. The DIP represented the body with upper and lower rigid segments with active joints at the hip and ankle. Their model contained two

eigenfrequencies that approximated the upper and lower limits of the main part of the anterior-posterior horizontal force power spectrum in human data. Their DIP model was able to achieve stable control using hip joint torque and no ankle torque.

Gunther et. al (2009) furthered their observations of upright standing showing that the motion at all leg joints contributes to balance control in humans, as opposed to just the ankle joint. This multi-joint coordination was seen in tight coupling of ankle and knee torque, antiphase kinematics of ankle and hip, and the inclusion of the higher frequency components (4-8Hz) of shank oscillations.

Furthermore, Gunther and Wagner (2016) improved the human balance model by analyzing the Triple Inverted Pendulum (TIP): lower legs, upper legs, and torso. Their TIP aimed to use stable balancing attractors using minimal sensor information and actuation complexity. Their model was able to replicate the mechanical energy eigenfrequencies present in human standing from 0.1 to 20Hz. They also were able to show that a low ankle joint stiffness was possible (below statically required values), when also coupled with an active hip torque balancing strategy. The increasing degrees of freedom for the representation of the human body from SIP to TIP demonstrates the necessary coordination of multiple joint torques to control the mechanical nature of standing balance.

1.3 Frequency Analyses of Mechanical Variables

To establish the frequency correlation of multiple mechanical variables, Zatsiorsky and Duarte (1999) first described that *CP* had two distinct frequency components: rambling (slow, <0.4 Hz) and trembling (fast, > 0.4 Hz). The rambling trajectory consisted of a spline interpolated path through the discrete *CP* locations observed at the instants when the horizontal force equaled zero, which corresponded approximately to the average Center of Mass (*CM*) horizontal trajectory. Trembling was described as the difference between the measured *CP* trajectory and the rambling trajectory. They determined that the magnitude of trembling was proportional to the horizontal force and that trembling was in phase with the horizontal force. Furthermore, in their following paper (2000), they presented that the power spectral density of the horizontal force was similar to the trembling but not the rambling trajectories. These observations indicate that, at higher frequencies (> 0.4 Hz), *F* varies in a constrained manner such that its orientation (primarily due to the horizontal component because the vertical component is nearly constant) and *CP* oscillate in phase. However, the precise nature of that relationship has yet to quantified.

Winter et. al (1998) reported that the average anteroposterior CP (*xCP*) was about 4ms delayed behind average *CM* locations, which they presented as evidence that reactive control of *CP* was not present (the time difference of 4ms could be considered negligible given their measurement resolution of 50ms for their kinematic data). They stated that a reactive control would induce at least a 150ms

lag of *CP* relative to *CM* and attributed the observed short delay of 4ms to the damping of the tuned mechanical system of the human body. Additionally, Wang et. al (2014) presented that standing bipedally and unipedally displayed high coherence between *CM* and CP for low frequencies (< 0.5 Hz). The coherence indicated the extent to which *CM* and *CP* are correlated.

The physical need for the average *CP* (over some time period more than 2 seconds) to be in phase and along the same vertical line of action as the average *CM* is displayed through the high coherence for the low-frequency variation of *CM* and *CP*. This physical necessity is due to the requirement that both the average horizontal force be zero, and that the torque about the *CM* is zero as well. This necessity is illustrated as followed: the average horizontal force is zero meaning that, on average, *F* is vertical. If that average vertical *F* were to be located offset from the average *CM*, there would an average torque about the *CM* that was non-zero, thus causing the whole body to pitch and eventually tip over. Winter et. al. and Wang et. al. presented data about the *CM*-CP relationship which solely simplifies the understanding of standing balance to translational control. There remains a need to understand how rotational control also affects standing balance, through the forces and torques acting on the body.

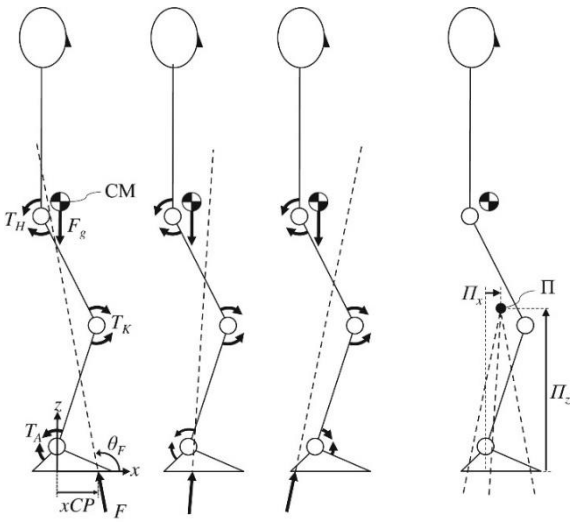

Figure 3 from Gruben & Boehm, 2012 shows the variation of *xCP* and *Fx*/*Fz* to create an IP near the knee when hip and knee torques are held constant. T_H, T_K, and T_A are the hip, knee, and ankle torque respectively. Π is the location of the Posture Specific Intersection Point

To understand how joint torques interact with a multi-segment body to produce *F*, Gruben and Boehm (2012) reported how the ratio of *Fx* to *Fz* covaries with *xCP* under various joint torque coordination constraints. They showed that a set of forces of the ground on feet, produced for a range of ankle torques at a given posture, are directed at a fixed point (intersection point, *IP*) located above the center of mass when joints above the ankle were held rigid by precisely controlling all joint torques. The joints above the ankle being rigid make the model equivalent to the Winter et. al. (1998) SIP model. Alternatively, when the hip and knee torques are instead held constant, these forces (of the ground on the feet) are instead directed at an *IP* near the knee (Figure 3).

1.4 Focus of Research

As previously described, great emphasis has been placed on creating mechanical models that attempt to explain the kinetic and kinematic characteristics of

unperturbed standing. Postural control requires the neural system to control joint torques in such a way as to modulate the force of the ground on the body (*F*) to ensure that the whole body does not fall down or fall over. Due to Zatsiorsky's evidence (Zatsiorsky and Duarte, 1999) of a high correlation between *Fx* and *xCP* in the higher frequency ranges (> 0.4 Hz), this study will focus on how the *F* vector contributes to both translational and rotational body motion. Specifically, it will characterize the observable behavior of unperturbed standing through the variables of *xCP*, *Fx*, and *Fz*.

1.5 Theory of Intersection Point *F* Control

The Intersection Point (*IP*) is the geometric representation of the covariation of *xCP* and F_x/F_z. This study will first determine if an *IP* provides a reasonable description of *F* variations. If a linear relationship exists between *Fx*/*Fz* and *xCP*, then the *F* vectors across time will intersect at a point. Such a relationship can be represented as in Equation 1. (Gruben & Boehm, 2012).

$zIP = xCP \,/\, (F_x/F_z)$ ..... eq. 1

where the *zIP* is the height of the *IP* (Figure 4).

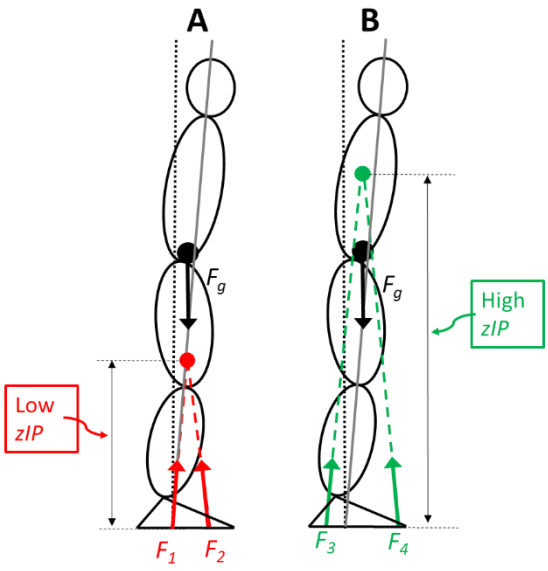

Figure 4: Panel A (Low *zIP*) and Panel B (High *zIP*) display human models pitched forward. The CMs are to the right of the upright *xCM* positions (indicated by vertical dotted black lines), and their whole body angular positions (slanted gray line) are clockwise from vertical.

This geometric relationship will occur when *xCP* and *Fx*/*Fz* are in phase with one another, meaning that a change in *xCP* is simultaneous with a proportional change in *Fx*/*Fz* and the slope of that relationship is z*IP*.

The location of the *IP* relative to the height of the *CM* has distinct behavioral outcomes. These can be illustrated for a forward pitched human in need of restored upright posture (Figure 4). The proportionality of *Fx*/*Fz* with respect to *xCP* determines the *IP* height (*zIP*). It is also possible for those variables to vary independently or in some other systematic pattern and not exhibit an *IP* at all (albeit still satisfying the constraints of average forces and torques consistent with standing). Thus, if an *IP* is observed it indicates a specific functional relationship among the joint torques (hip, knee, ankle) which can alternately be expressed equivalently in force space (*Fx*, *Fz*, *xCP*).

If an F_4 (*Fx* leftward, *Fz* upward) is part of a set of *F* with an *IP* above the *CM* (Fig. 4A), it will cause the body to have a translational acceleration to the left and counter-clockwise angular acceleration, both of which act to restore upright posture. If an F_2 (*Fx* to the left, *Fz* up) is part of a set of *F* with an *IP* below the *CM* (Fig. 4B), it will cause the body to have a translational acceleration to the left as

before but will have a clockwise angular acceleration. This motion combination acts to reposition the *CM* back to the desired upright posture position but also acts to rotate the whole body further in the direction of the initial postural perturbation. Due to the constraint of keeping the foot stationary, this also requires the body to flex at the hip and/or knee joints. These two classes of behavior demonstrate the effect of *IP* height on upright posture, namely, an *IP* below the *CM* will not restore both translational and rotational motion necessary to respond to rigid body tip but an *IP* above the *CM* will. Conversely, if the body posture away from upright standing is not that of a simple tip but instead, has *CM* shifted rightward and whole body angular position rotated counter-clockwise, this infra-*CM* strategy could be helpful in restoring upright posture.

1.6 Aim and Hypothesis

Interestingly, humans have the ability to produce many variations of *F* due to a multitude of joint torque combinations, so the purpose of this study is to investigate if the neural system employs some particular coordination strategies and to evaluate how those variations relate to the mechanical requirements of standing. This thesis will specifically explore the presence of *IP F* behavior in unperturbed standing by analyzing how *xCP* and *Fx*/*Fz* covary. Based on pilot data, we hypothesize that humans have a preference to direct *F* at intersection points (*IP*s) and that the location of those *IP*s relate to the goals of ensuring desired translational and rotational motion of the body.

1.7 Significance

This characterization of muscle coordination has broad application. It can be used in the design of humanoid robotic control and the improvement of the control systems for bionic prostheses. If the *IP* control is shown to be a fundamental way humans control unperturbed standing, then alterations in the control may provide insight into the balance disruption and prospective novel therapies associated with neural disorders such as stroke and Parkinson's disease

2. METHODOLOGY

2.1 Introduction

The mechanical variables of *Fx*, *Fz*, and *xCP* were recorded on a calibrated custom force plate during unperturbed standing in humans without a history of musculoskeletal or neurological disorders that could affect standing. A frequency analysis of these variables was performed to quantify coordination.

2.2 Force Plate Design and Calibration

Figure 5 displays the Custom force plate

A custom force plate (Fiure 5) was designed and built instead of a conventional force plate due to its precision, ease of adjustment and calibration, and high horizontal force sensitivity. This force plate consisted of a rigid aluminum plate attached to 4 vertical (440 N capacity) and 3 horizontal (two 44N and one 440 N capacity) uniaxial force sensors, using a configuration similar to that previously published (McLeish and Arnold, 1972). The sensors were supported by a rigid frame. Each of the seven forces, supporting the plate, was provided through long tensile or compression members that do not support moments at each end. These members ensured that the sensors are loaded

uniaxially, centered, and aligned with their loading axis. The force in each sensor (Measurement Specialties, Berwyn, PA, FC2231) was calculated from measured voltage and calibration coefficients determined from static loading of each sensor before assembly. The geometry of the sensor array was used to calculate the center of pressure (CP).

A calibration process was performed on the custom force plate to estimate its measurement error. The process involved using known vertical weights, horizontal forces, and point contacts. The mean error of *Fx, Fz, xCP* were 0.229N, 0.590N, and 0.00195m.

2.3 Experimental Design

Ten healthy adults participated in this experiment (4 female, ages 18 to 53 years). The subjects were only included if they were void of any neuromuscular diseases or current musculoskeletal injuries. Participation was voluntary, written consent was obtained, and the protocol was approved by the University of Wisconsin Institutional Review Board. Measurements were recorded at the vertical distance from the floor to the palpated ankle joint (lateral malleolus), knee joint (lateral epicondyle of femur), hip joint (greater trochanter of femur), and shoulder joint (greater tuberosity of humerus), as well as total body height.

The participants performed quiet standing with arms at their sides on the custom force plate. The participants stood with both feet together for 50 seconds while focusing on an ‘X’ diagram placed at head height 1 m anterior. Custom software

recorded at 1000Hz in sagittal-plane *F* (*Fx, Fz*) and *xCP* (+x posterior, +z superior). The *xCP* and *Fx*/*Fz* were bandpass filtered (zero lag, 2nd order Butterworth) in 20 bins with 0.5 Hz width (0 to 0.5 Hz, 0.5 to 1 Hz, …, 9.5 to 10 Hz). Half Hertz width was chosen for the bandpass width to give reasonable power within each band.

The principal component of the relation between *xCP* and *Fx*/*Fz* for each frequency bin was calculated to determine the height of the *IP*. The *IP* height was plotted against frequency for each trial (Figure 11). Also, the power spectrum was calculated for *xCP* and *Fx*/*Fz* where the area under each curve was normalized to equal 1 (Figure 12). The *variance accounted for* (VAF) by the first principal component was calculated to assess the ability of the intersection point to describe the relationship between *xCP* and *Fx*/*Fz* (Figure 13).

2.4 Mechanical Validation of *IP* Behavior

Force plate measurements for various non-human rigid bodies were taken to validate the frequency analysis and to understand further the *xCP* and *Fx*/*Fz* covariation in different mechanical systems that should exhibit *IP*s.

Rocking masses: Gruben & Boehm (2012) previously showed that a rigid body, rocking infinitesimally back and forth, has a linear relationship between *xCP* and *Fx*/*Fz* which can be represented geometrically as the support force line-of-action being always constrained to pass through a fixed point located above the *CM*. An 11kg mass was set atop a smoothly

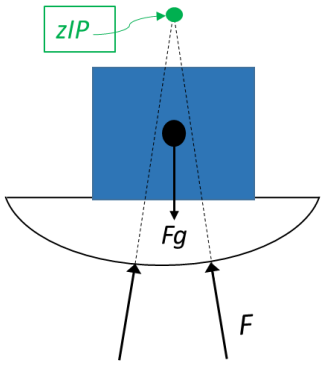

Figure 6 displays the Rocking mass

curved base (0.35m radius) and was rocked with a small initial rotational motion (Figure 6). Additionally, a water tube (1.75m tall and similar moment of inertia to humans) was attached to a slightly curved base (near infinite radius). The rocking water tube gives insight to potential *IP* behavior despite the lack of internal rigidity (there is some space for the water to move inside the tube).

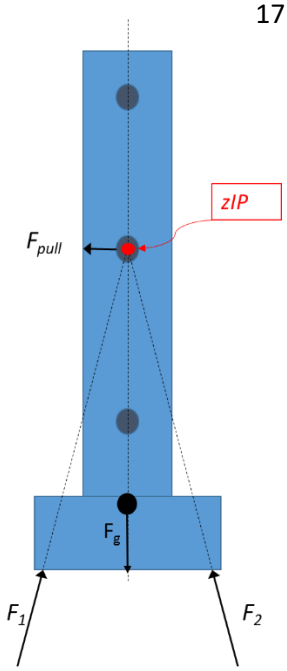

Figure 7 displays the Vertical Pole

Horizontal force applied to vertical pole: rigid aluminum structure 2m tall was attached to a rigid and heavy (80kg) base (Figure 7). Strings were attached to the pole at 0.5, 1.0 and 1.5 m high, pulled taut horizontally and passed around pulleys on a separate fixture (pulleys at the same vertical height as string attachment to ensure that each string is horizontal). *F* in the strings (one at a time) was oscillated in magnitude manually at about the same frequency for 10 s. The force magnitude was below the force necessary to cause the pole to tip or bend or its base to slip. The mechanics of the set-up ensured that the force of the ground on the pole intersects at the intersection of the force of gravity and the horizontal string, thus replicating the expected *F* variation of humans.

Frequency analyses were applied to the use the *xCP*, *Fx*, *Fz* data to verify the presence of *IP* in these systems, and to validate the method of determining *IP* and accuracy of the custom force plate.

3. RESULTS

Figures 8 and 9 show a 50s duration of *xCP* and *Fr (Fx/Fz)* of a representative trial of unperturbed standing for one of the subjects. Figure 10 displays the raw and filtered data (1.5-2Hz) of the variation *xCP* with *Fr* from the representative data. The raw data appeared as a cloud of data that has large variation in both *xCP* and *Fr*. The filtered data appears as a tighter variation (closer to a straight line) where for a small variation of *xCP*, there is a large variation of *Fr*.

Principal Component Analysis (PCA) was used to determine the fit of the two signals (how they covary) where the inverse of the slope of that fit is the height of the *IP*. To create an IP, *xCP* and *Fr* need to be linearly related (form a straight line) which can be showed as its first principal component. The fitted line of the raw data showed the dominant slow variation for *xCP* and *Fr* that exists in standing that gives a high IP of 6.15 as a multiple of body height (body height = 1.68m). The fitted line of the filtered data showed the dominant faster variation that gives a lower IP of 0.65 as a fraction of body height (slightly above average CM height).

The *IP* height (fraction of body height) was then plotted against frequency in Figure 11 where it progressively decreased with increasing frequency. The mean and individual IP heights were displayed in the figure. The *CM* height for an average human (horizontal line) was 0.56 of body height (Croskey, Marguerite I., et al., 1922). The low-frequency average IP Height (0-1.5 Hz) was above the *CM*, and the higher frequency IP Heights (above 2 Hz) was below the *CM* height. The lowest frequency *IP* heights were not shown in this graph due to its high

magnitudes; most of the heights ranged from 6 to 49.1 as a multiple of body height (one subject had an IP of -27.5).

To demonstrate how well *xCP* and *Fr* created an *IP* for each frequency, the variances accounted for (VAFs) were plotted in Figure 12. An *IP* that describes the variation in *xCP* and Fx/Fz well gives a VAF (variance accounted for) value near 1. A VAF of 0.5 indicates that the data set is best fitted by a circle and a VAF of 1 shows that the data set is best fitted by a straight line.

Figure 13 shows the Normalized Mean Power of *xCP* and *Fr* vs. frequency (Hz). Much of the power present in the *xCP* of quiet standing is at lower frequencies (85.3% of *xCP* power < 0.25 Hz), whereas *Fr* has much less of its power in this range (1.9% of *Fr* power < 0.25 Hz range). Some of the power (14.5%) present in the *xCP* is between 0.25 and 2Hz whereas much of *Fr* power (75.0%) is in this range. *xCP* and *Fr* have 0.13% and 6.63% respectively of total power respectively above 4 Hz.

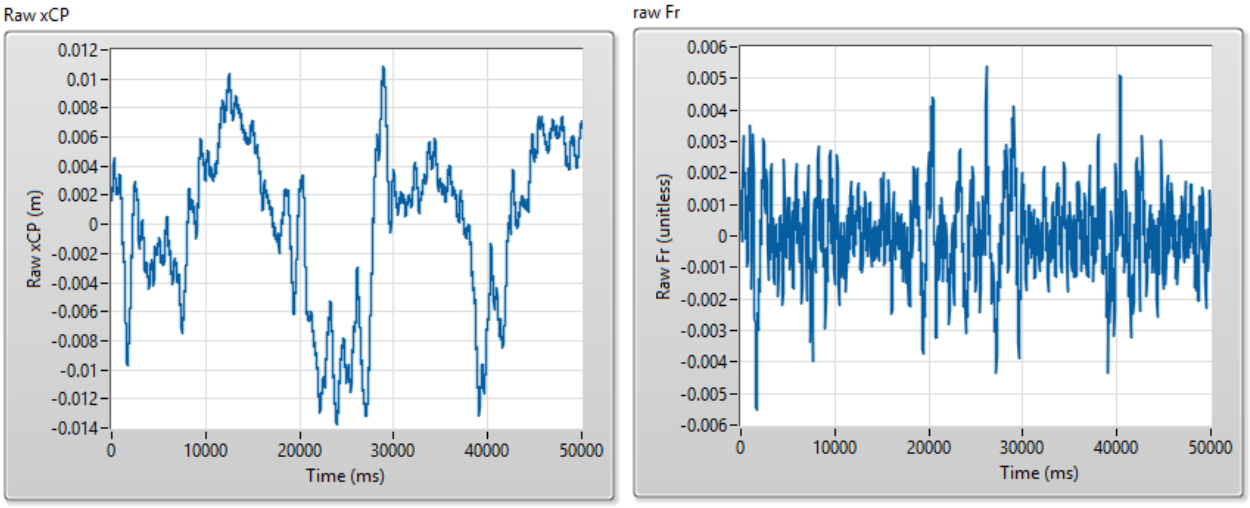

Figure 8 and 9 shows raw signals of *xCP* and *Fr* respectively vs. time for sample human.

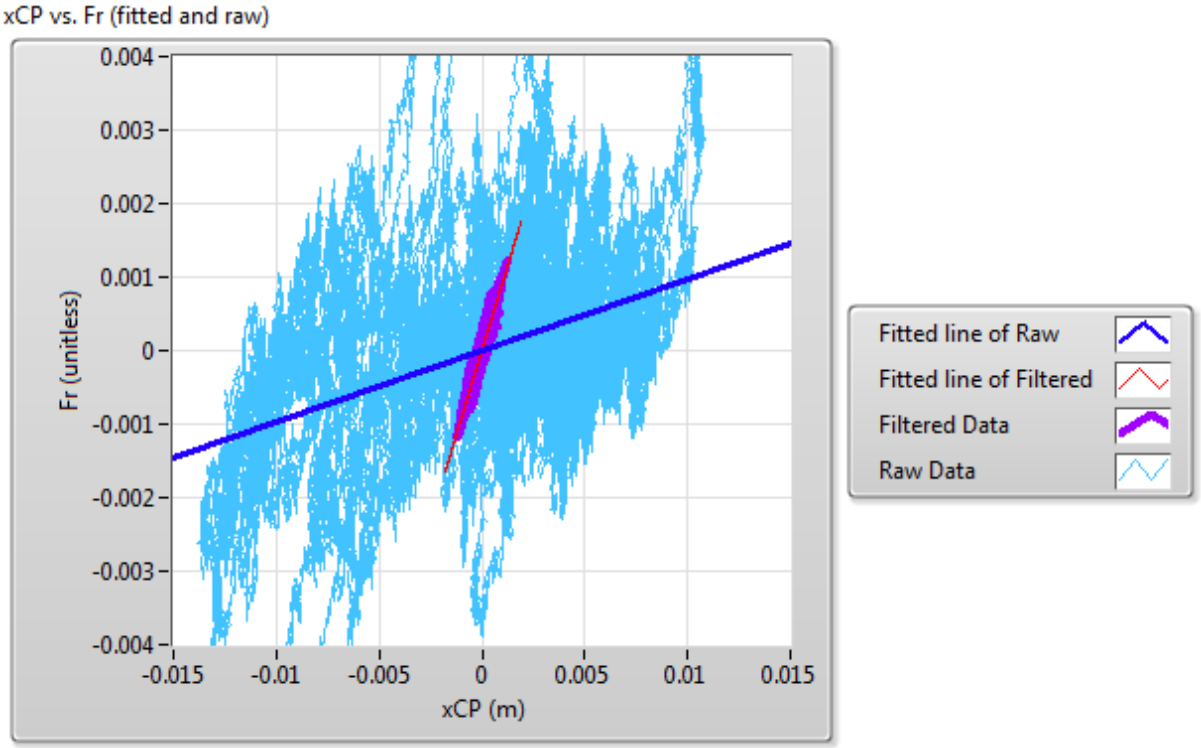

Figure 10 shows *xCP* vs. *Fr (Fx/Fz)* for signals in Figures 7 and 8. The filtered data includes only the data in the frequency band of 1.5-2 Hz. The Fitted lines of Raw and Filtered show the 1st Principal Component for Filtered and Raw data. The fitted line of the raw data shows the dominant slow variation for *xCP* and *Fr* that exists in standing that gives a high *IP* of 6.15 as a multiple of body height (body height = 1.68m). The fitted line of the filtered data shows the dominant faster variation that gives a lower *IP* of 0.65 as a fraction of body height (slightly above average *CM* height).

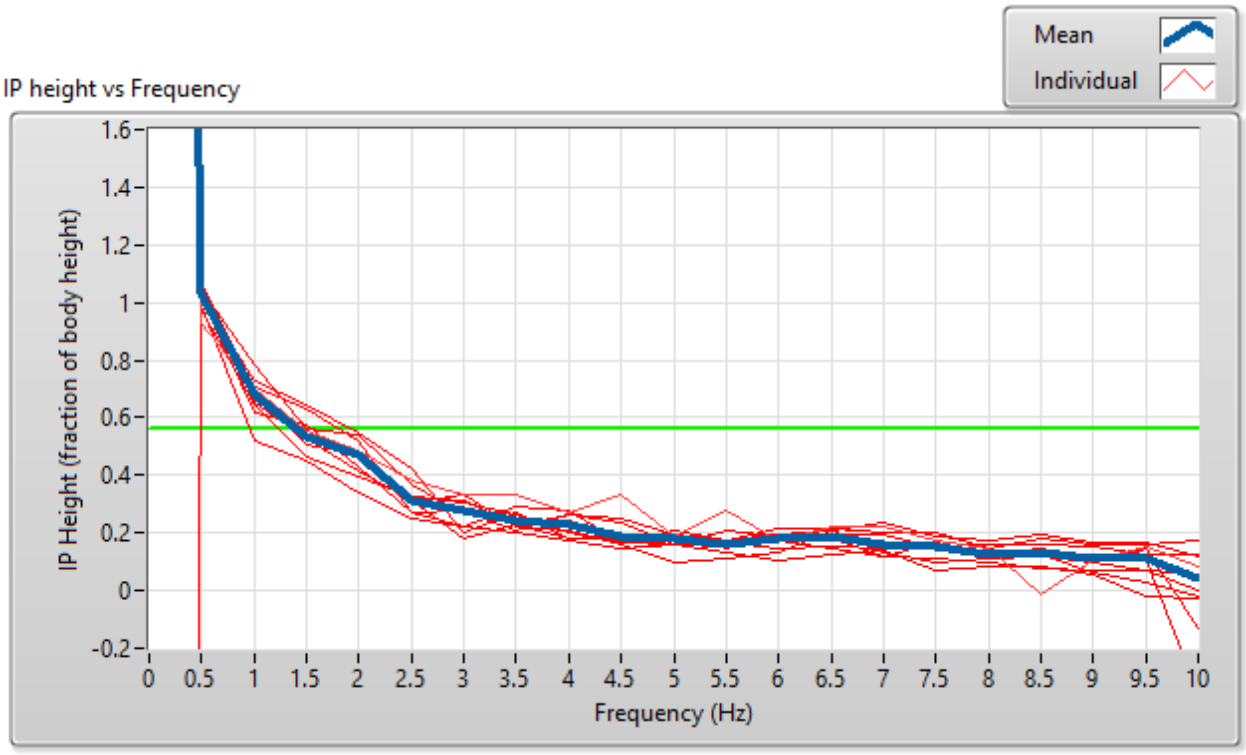

Figure 11: The *IP* height (fraction of body height) progressively decreases with increasing frequency. The thicker line represents the mean IP height across frequency for 10 subjects. The *CM* height for an average human (horizontal line) is 0.56 of body height (Croskey, Marguerite I., et al., 1922). The low-frequency average *IP* Height (0-2 Hz) is above the *CM*, and the higher frequency *IP* Heights (above 2 Hz) is below the *CM* height. The lowest frequency *IP* heights are not shown in this graph; most of the heights ranged from 6 to 49.1 as a multiple of body height (one subject had an *IP* of -27.5).

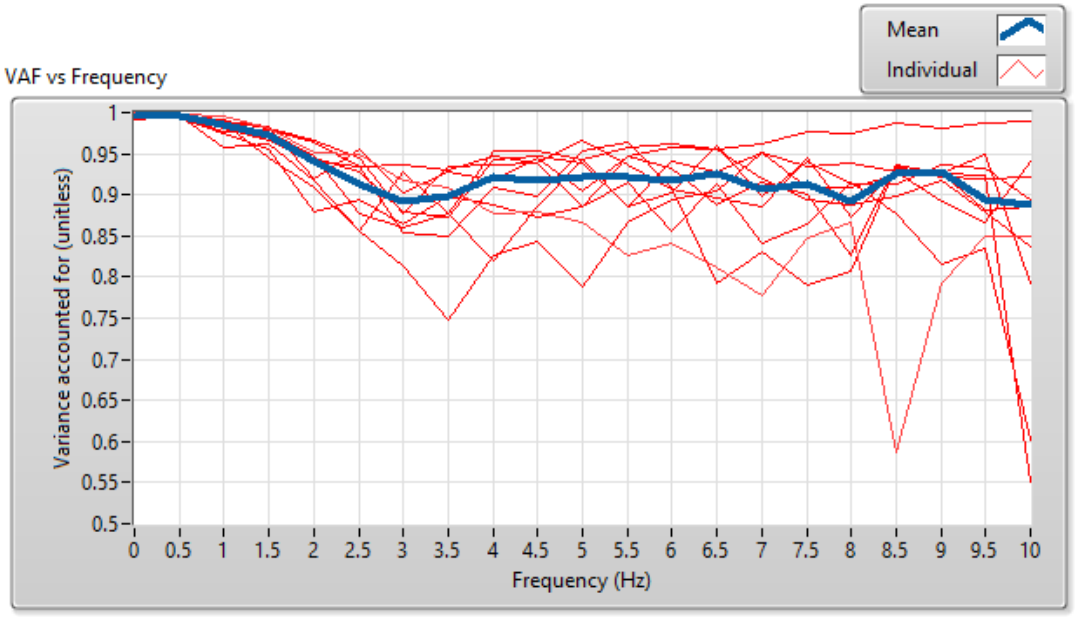

Figure 12: An *IP* that describes the variation in *xCP* and *Fx*/*Fz* well gives a VAF (variance accounted for) value near 1. The thicker line represents the mean VAF across frequency for 10 subjects. A VAF of 0.5 indicates that the data set is best fitted by a circle and a VAF of 1 shows that the data set is best fitted by a straight line.

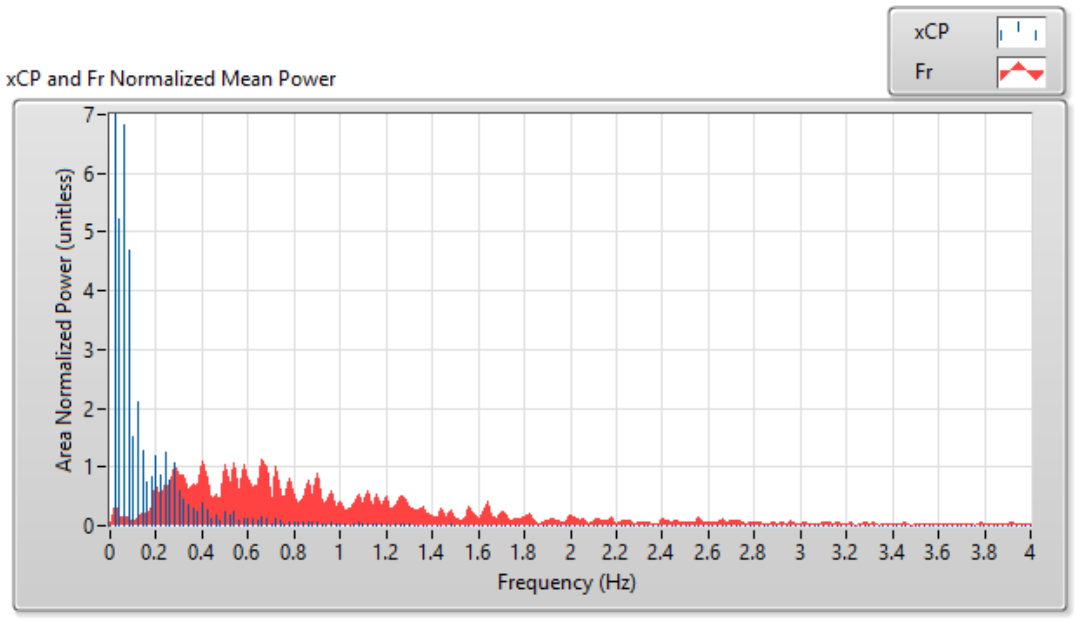

Figure 13 shows the Normalized Mean Power of *xCP* and *Fr* vs. Frequency (Hz). *xCP* has 85.1% of total power between frequencies of 0 and .25 Hz due to slow body sway. Fr has 75.0% of total power between frequencies of 0.25 and 2 Hz. *xCP* and Fr have 0.13% and 6.63% respectively of total power respectively above 4 Hz.

5. DISCUSSION

Within the mechanical constraints of the human body, the neural system controls the joints torques in such a way as to modulate the force of the ground on the body (*F*) to ensure that the whole body remains standing. Humans have the ability to successfully stand using many variations in *F* (magnitude, direction, and location) due to the flexibility with which joint torques can be combined. The results demonstrated that the neural system employs a particular coordination that can be represented as intersection points of the *F* lines of action. The presented *IP* behavior provides some insight into how humans maintain translational and rotational balance.

5.1 Frequency Content of *IP* behavior

Much of the power present in the *xCP* of quiet standing is at lower frequencies (85.3% of *xCP* power < 0.25 Hz), whereas *Fr* has much less of its power in this range (1.9% of *Fr* power < 0.25 Hz range). In this frequency band, variation in *xCP* is much larger than in *Fr* variation (Zatsiorsky and Duarte, 1999) so the *F* vectors are mostly parallel to each other which could be represented as an *IP* at infinite height (+ or −). Such *F* vectors primarily serve to cause rotational acceleration of the whole body and produce little translational acceleration. The small amount of horizontal force that is present is responsible for the slow translation of the *CM*

fore and aft. The rotational acceleration produced by the shift in CP away from directly below the *CM* while the force remains nearly vertical serves to modulate angular motion of the body as a whole.

For the frequency band 1.5-2 Hz, variation in *xCP* and *Fr* gives *F* vectors that are directed towards points arbitrarily close to *CM* height (Figure 11). Such *F* vectors primarily serve to cause mainly translational acceleration of the whole body and produce little rotational acceleration. The horizontal force produced is responsible for larger movements of the *CM* fore and aft.

For frequencies above 2 Hz, the *IP* heights were below the *CM*. This tends to differently affect the translational and rotational aspects of whole body accelerations (translational posture is restored but rotational posture is not). However, such behavior provides a mechanism for rapid translational acceleration because the force ratio is larger for a given *xCP* thus generating a larger horizontal *F*. If *F* was always constrained to be directed at an *IP* located above the *CM*, a large horizontal force would require a large shift of the CP. Due to the limited foot length, the CP can only shift to the toe or heel. With a supra-*CM IP*, this would place a significant constraint on the magnitude of the horizontal force and thus speed at which *CM* horizontal location could be corrected.

By altering the coordination to an infra-*CM IP*, the horizontal force can be much larger while keeping the CP within the foot length. The direction of such a *F* causes angular acceleration that tips the body away from upright. While the feet are fixed on the ground, this whole body angular motion occurs due to a large

head-arms-trunk rotation. In this way, rapid *CM* translation can reposition the *CM* back to the original position at the expense of ending up in a hip-flexed or knee-flexed posture. The supra-*CM* coordination can then be used to restore whole body angular orientation to upright, while not disrupting horizontal *CM* position.

5.2 Relation of *IP* behavior in Torque Control and Fall Recovery

The strong linearity of *xCP* vs. *Fr* reveals that there is specific control of the hip and knee torques relative to the ankle torque. The low-frequency *IP* (below 2Hz) is above the *CM* which can be viewed as the inverted pendulum control where the hip and knee torque are controlled to keep the respective joints approximately rigid while the ankle torque primarily acts to shift the CP and pitch the whole body fore/aft. For a given joint configuration, only one specific z*IP* corresponds to the whole body being exactly rigid. The other supra-*CM* z*IP* values correspond to slight modifications of that configuration. At higher frequencies, the height of the *IP* decreases due to the control switching to a state where hip and knee torque are being modulated in a way that does not keep the respective joints rigid. As reported for a simulated standing human, holding the hip and knee torques constant results in a z*IP* that is near the knee (Gruben, K. and Boehm, 2012).

Various balance recovery strategies people use when preventing a fall have been quantified (Cheng, K, 2016). The subjects had to keep their feet stationary and recover their upright posture after being released from a tether, previously

holding them in a leaned forward posture. The various *IP* heights we observe are consistent with their results in which the released person begins to fall but initially corrects their *CM* translation with a brief high magnitude horizontal force (high frequency, low z*IP*) that results in the torso rotated forward due to hip flexion. The high-frequency behavior observed in the present study yielded a low *IP* height which is consistent with a large horizontal force coupled with a torque about the *CM* that pitches the body forward even further. At slower frequencies, the *IP* is higher and the *F* can provide the torque about the *CM* necessary to rotate the body back toward upright without with little change to *CM* location. Thus, all participants demonstrated behaviors that accelerated both the translational and rotational degrees-of-freedom back toward upright but accomplished these two tasks at distinct frequencies using distinct coordination strategies.

The striking finding is that humans could be exhibiting similar coordinative strategies during the two tasks of fall recovery and quiet standing. While leaned-posture recovery was not evaluated in this thesis, it seems likely that the coordination used for the initial response involved an infra-*CM IP* that is the same coordinative strategy that was exhibited at high frequencies during quiet standing. Likewise, the secondary righting response appears to use the same coordination as observed for quiet standing at low frequencies. This conservation of coordinative strategies across tasks has been reported previously across walking and pedaling tasks (Zehr, E. Paul, et al., 2007) and across walking and non-balance tasks (Schmidt, M, 2003 and Gruben, K and Boehm, W, 2014).

5.3 Comparison of Human Standing Behavior to other Mechanical Systems

In Appendix C, the rocking mass, water tube, and the vertical pole being pulled horizontally give purely mechanical examples of the presence of *IP* behavior. The rigid rocking mass (Figure 26) gave a supra-*CM IP* for the frequency at which it rocked (around 1 Hz). The higher frequencies gave very high and low *IP* heights but possessed little power for *xCP* and *Fr* and had VAFs generally below 0.9. The low powers and VAF indicate that the *xCP* and Fr covariation was not relating to a straight line, thereby, not having an *IP*s for those frequencies.

The rocking water tube (Figure 26) also gave a supra-*CM IP* for the frequency at which it rocked (around 1.5 Hz) where there was high power for *xCP* and *Fr*. The water tube was used because it had a similar height and moment of inertia of an average human. There was also some power at 3 Hz that gave similar *IP*s and had a high VAF which may correspond to the higher frequency movement of the water in the tube. The *IP*s for the frequencies above 6Hz gave high and low *IP* but had a VAF below 0.9, indicating a poorer fit of *IP* behavior.

The vertical pole (Figure 27) being pulled horizontally gave *IP* heights close to the pulling height with a frequency about 2.3Hz. There were also some harmonic lower magnitude frequencies present in the *xCP* and Fr at about 4.7 and 6.9Hz. These harmonics may be due to the bending modes of the pole, but the 6.9 Hz harmonic gave a consistent *IP* around 0.4m for all three pull heights. These results may be some evidence of the natural harmonic bending of a body creating an *IP* behavior

due to systematic variation of *xCP* and Fr. There were VAFs close to 1 for *IP*s with frequencies below 7Hz.

These mechanical systems show that the custom force plate and frequency analyses are sufficient for detecting *IP* behavior. They also show that a VAF below 0.9 indicates the poor fit of *xCP* and *Fr* to create an *IP*.

5.4 Other Analyses to understand the covariation of *xCP* and *Fr*

Pilot Data for this thesis involved using Wavelet analyses to display the time-frequency coordination of *xCP* and Fr to give *IP* behavior. In Appendix A, LabVIEW's Wavelet package showed similar results of *IP* behavior (Figure 23) as what is shown in main results in the thesis (Figure 11). The similarities involve the inverse relationship of *IP* height and frequency with high *IP*s for low-frequency variation and low *IP*s for high-frequency variation of *xCP* and *Fr*. The results of this wavelet analysis differed with respect to an average lowest frequency *IP* being close to 1.75m (close to average body height) as opposed to a near infinite *IP* height for the thesis results. Also, the higher frequency *IP*s tended to 0.5m rather than to 0m as seen in the thesis results.

The aforementioned differences of the thesis and pilot data could be primarily due difficulty with comparing the phase difference of the *xCP* and *Fr* signals. These two signals were independently processed by LabVIEW's Wavelet Package where their individual phasing was compared to the phasing of the Gabor Wavelet. Their

phasing depended on the FFT (Fast Fourier Transform) magnitude of the real and imaginary components, and how much larger/smaller it is than the FFT of the Gabor Wavelet. It was mathematically incorrect to find the phase difference of *xCP* and *Fr* by finding the subtraction of the frequency transformed signals due to the functions that govern Fourier Transforms.

The correct way to quantify the phase shift was to perform a cross-correlation of the two signals (Francesco, B. and Ferrini, G., 2012). In need of this cross correlation, Matlab's Wavelet Coherence was used, as shown in Appendix B. The Coherence (Figure 25) showed that throughout the main duration of the standing trial, the frequency band 0.25 - 4 Hz of *xCP* and *Fr* was mostly in phase (high coherence). Despite the advantages of this method, it was unable to give the individuals magnitudes of *xCP* and *Fr* for the frequency content that is in phase, which is necessary to obtain the *IP* height.

All in all, the Wavelet analyses proved useful in giving an insight of in-phase nature of certain frequency bands through time for *xCP* and *Fr,* but its limitations promoted the use of the frequency filters and PCA methods used in the methods of this thesis to quantify *IP* behavior in standing balance.

5.5 Future Application of *IP* Research

IP behavior occurs due to the interaction of the mechanical and neural systems, so mechanical perturbations, diseases, and disabilities will impact the system as

quantified with this method. Future studies will investigate the change of this coordination with mechanical perturbations like brief horizontal force and standing on a small support. Other studies will focus on understanding the differences of *IP* behavior in populations with balance problems secondary to neuromuscular diseases such as stroke and Parkinson's disease. The mechanism for control of translational and rotational motion through the use of the foot force vector, characterized in this study, has broad application for evaluation, training, and design of bipedal postural tasks.

5. CONCLUSION

In light of the need in current literature for a description of the translational and rotational control of standing balance, this thesis presented a coordination of the mechanical variables center of pressure and the ratio of horizontal and vertical forces to create an Intersection Point behavior. This frequency dependent behavior demonstrates a simplified representation of how the neuromuscular coordination strategies control the force of the ground on the body to maintain upright standing balance.

6. APPENDICES

APPENDIX A

This section displays how the original pilot data from one subject was used to understand the utility of wavelet analysis, and how *xCP* and *Fx*/*Fz* was processed to find *IP*. Intersection Point height (z*IP*) was obtained by dividing the magnitudes of the *xCP* by *Fx*/*Fz* for each time and frequency windows using the LabVIEW's Wavelet Package. The z*IP* values were selected only for those times and frequencies where the magnitude in each of the signals is above 0.0001 (m for *xCP* and unitless for *Fx*/*Fz*) and the phase difference of *xCP* and *Fx*/*Fz* is close to 0 (within 5 degrees). For the selected times, the average of all *IP* heights at each 0.2 Hz increment was calculated from 0.2 to 10 Hz.

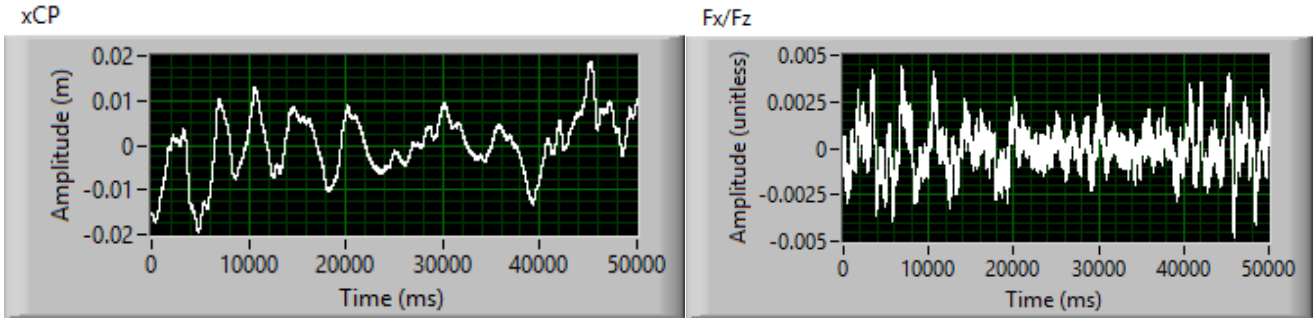

Figure 14 and 15 shows *xCP* and Fx/*Fz* respectively vs. time for sample human

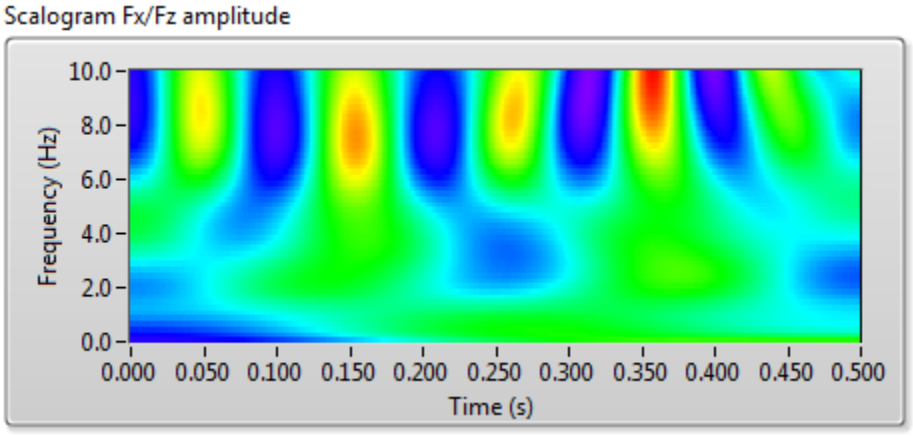

Figure 16

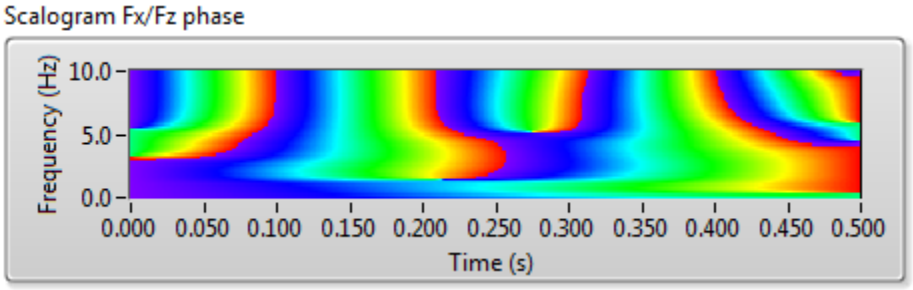

Figure 17

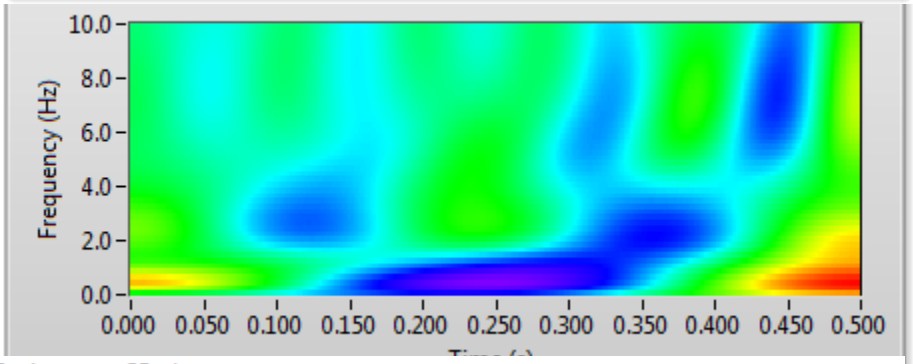

Figure 18

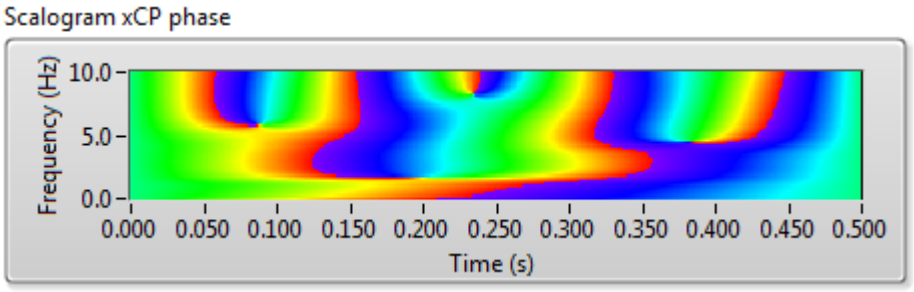

Figure 19

Figures 16, 17, 18, and 19 show amplitude and phase (in color) vs. Frequency (Hz) and Time (s). Red corresponds to the highest magnitude/phase. Blue corresponds to the lowest magnitude/phase. All Scalograms show data for 0.5 s because the entire data of 50s were broken

up into 0.5 s blocks due to the memory limits and computational burden of the high-resolution Wavelet Analysis (1 ms time intervals, 0.2 Hz frequency windows).

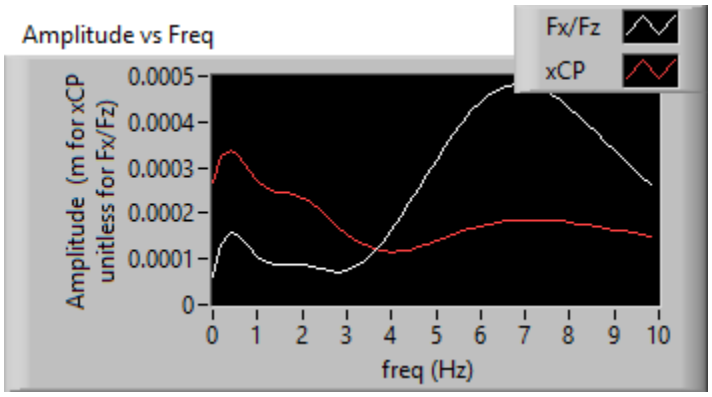

Figure 20 shows the Amplitude of *Fx/Fz* and *xCP* vs. Freq for one-time interval (1 ms)

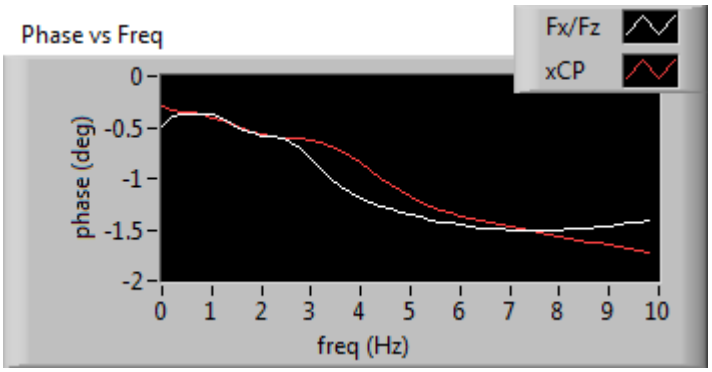

Figure 21 shows the Phase of *Fx/Fz* and *xCP* vs. Freq for one-time interval (1 ms)

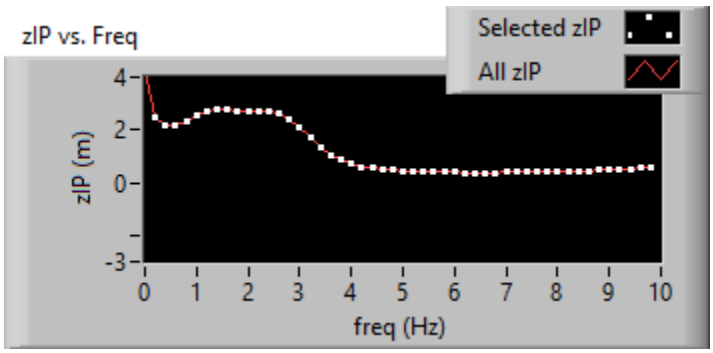

Figure 22: z*IP* vs. Freq of the *xCP* and *Fx*/Fz that had above 0.0001 magnitudes and were within -5 and 5 deg phase difference (Selected z*IP*) and all of the z*IP* for one-time interval (1 ms).

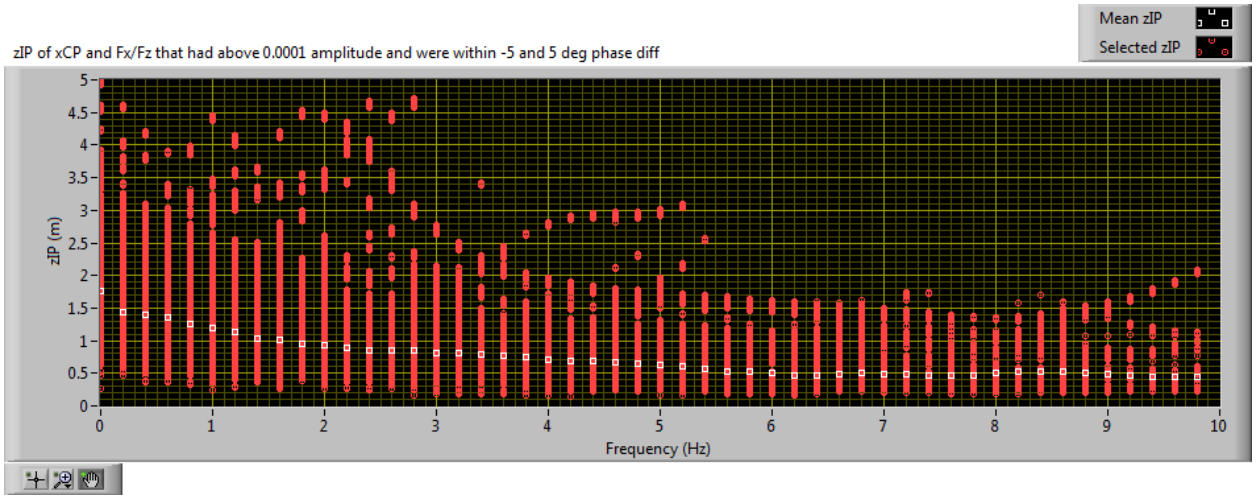

Figure 23: z*IP* vs. Freq of the *xCP* and *Fx*/*Fz* that had above 0.0001 magnitudes and were within -5 and 5 deg phase difference (Selected z*IP*) and mean z*IP* for the entire data set (50s). Red dots indicate the selected z*IP* across individual times for one subject.

APPENDIX B

This section displays how a sample *xCP* and *Fr* was analyzed using the Matlab continuous Wavelet Coherence Package.

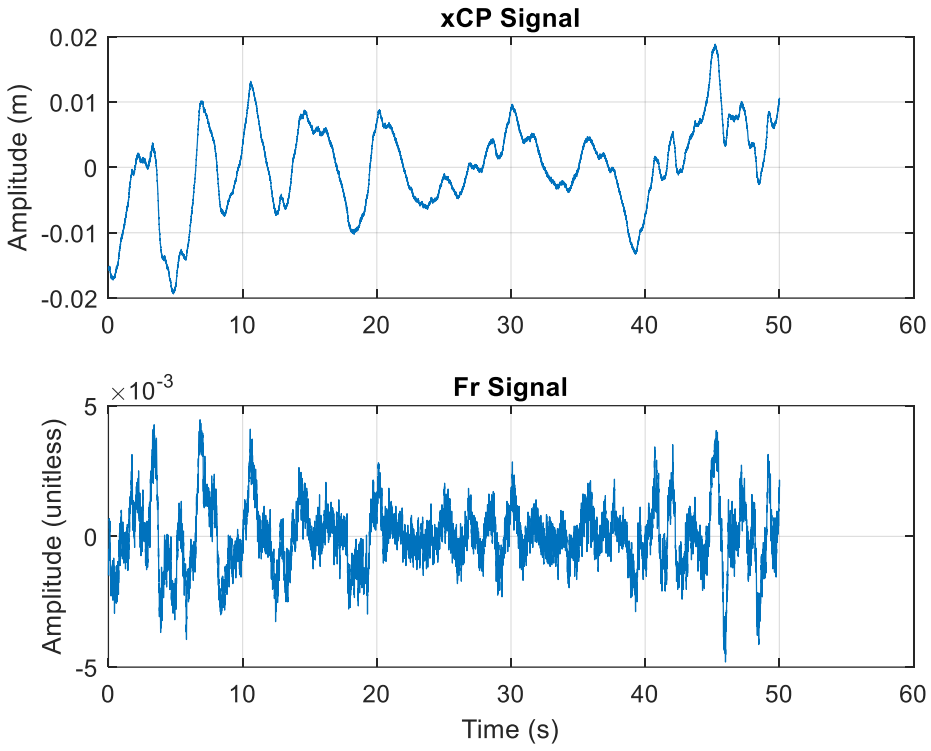

Figure 24 shows the *xCP* and *Fr* signals from one representative subject

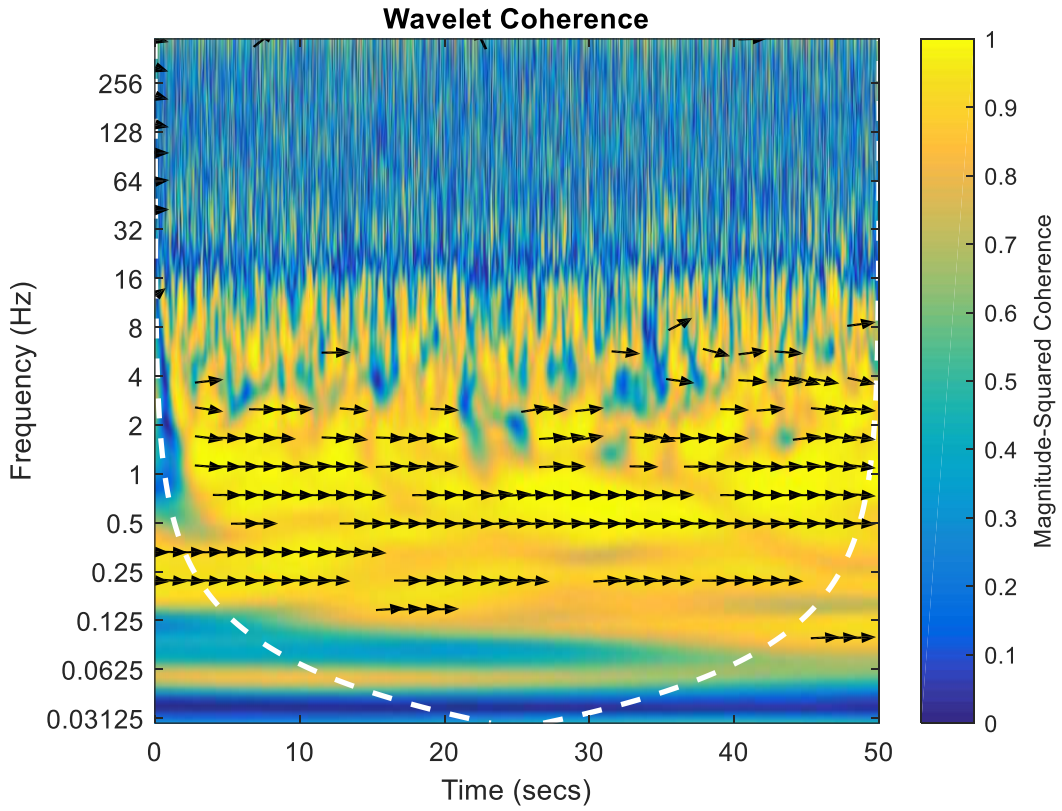

Figure 25 shows the results of a wavelet coherence analysis on the signals of *xCP* and *Fr* from figure 22. The arrows indicate the phase shift between the two signals where a horizontal arrow indicates no phase shift and a vertical arrow indicates and 90-degree phase shift. The inside of the white dashed U-shaped curve (cone of influence) shows the data that is not negatively affected by the filtering process.

APPENDIX C

These results display the *IP* behavior of various mechanical systems.

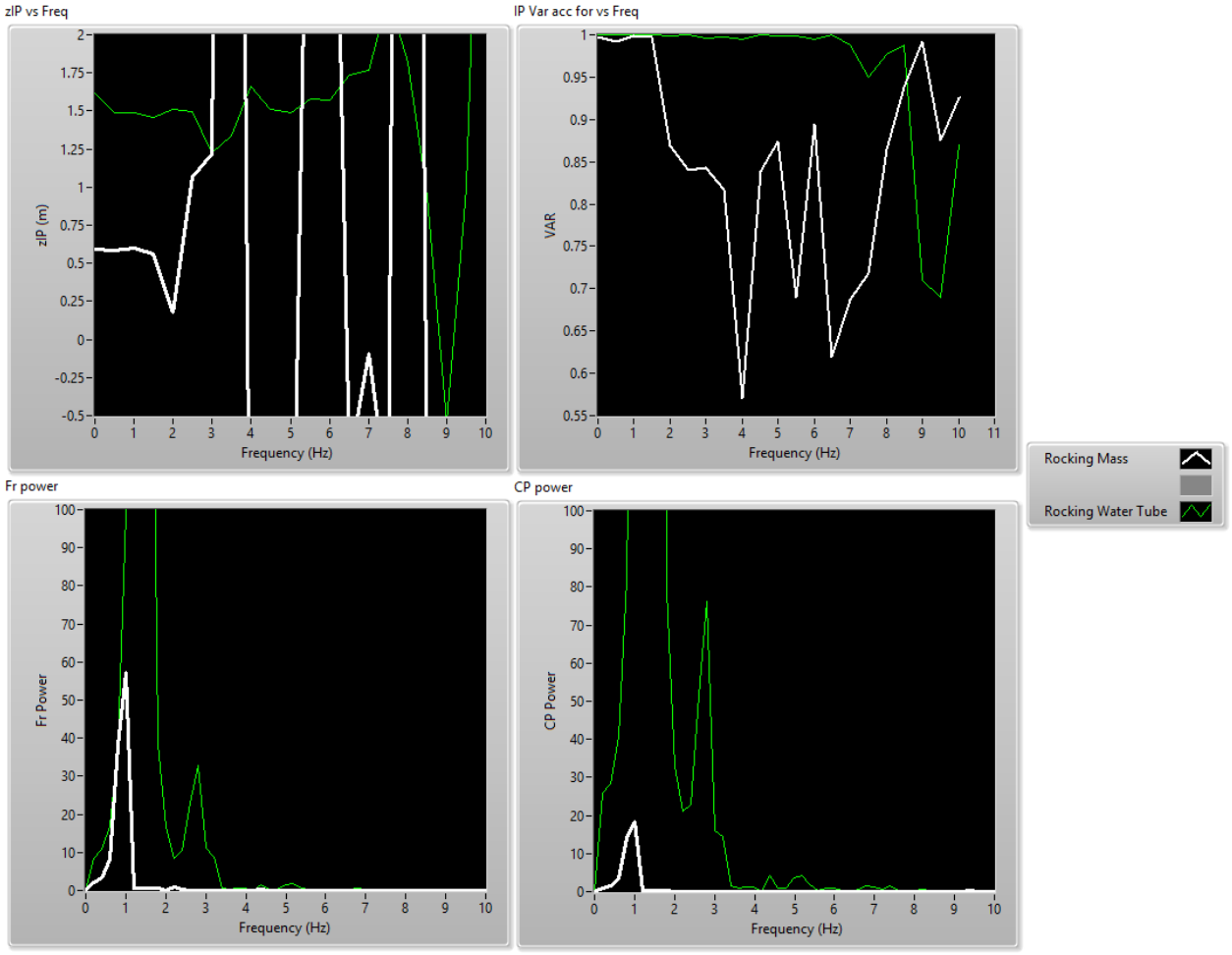

Figure 26: The *xCP* and Fr signals from the Rocking (solid) mass and a Rocking water tube. The rocking mass had a dominant frequency for *xCP* and *Fr* of around 1Hz which gave an *IP* height of 0.6m with a VAF close to 1. The rocking water tube had a dominant frequency for *xCP* and Fr of around 1.5 and 2.6Hz which gave an *IP* height of 1.5m with a VAF close to 1.

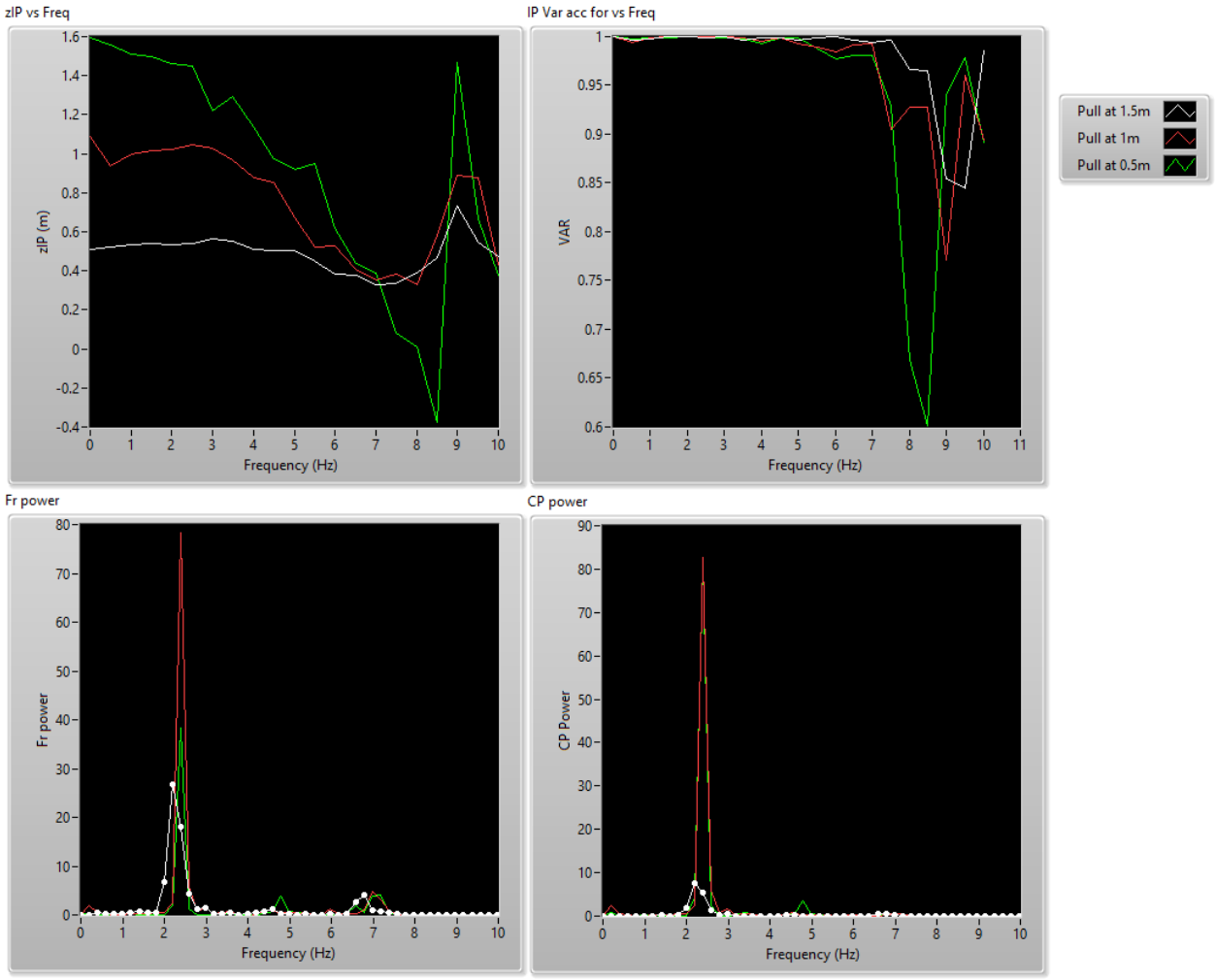

Figure 27 show the *xCP* and Fr signals from the vertical pole being pulled horizontally at 1.5, 1, 0.5m. All of the pulls had a dominant frequency for *xCP* and *Fr* of around 2.25Hz which gave an *IP* height close to the pulling height with a VAF close to 1.

7. REFERENCES

1. Otten, E. "Balancing on a narrow ridge: biomechanics and control." *Philosophical Transactions of the Royal Society of London B: Biological Sciences* 354.1385 (1999): 869-875
2. Zatsiorsky, Vladimir M., and Marcos Duarte. "Instant equilibrium point and its migration in standing tasks: rambling and trembling components of the stabilogram." *Motor Control* 3.1 (1999): 28-38.
3. Zatsiorsky, Vladimir M., and Marcos Duarte. "Rambling and trembling in quiet standing." *Motor Control-Champaign* 4.2 (2000): 185-200.
4. Winter, David A., et al. "Stiffness control of balance in quiet standing." *Journal of Neurophysiology* 80.3 (1998): 1211-1221.
5. Wang, Zheng, et al. "The degrees of freedom problem in human standing posture: collective and component dynamics." *PloS One* 9.1 (2014): e85414.
6. Gruben, Kreg G., and Wendy L. Boehm. "Mechanical interaction of center of pressure and force direction in the upright human." *Journal of Biomechanics* 45.9 (2012): 1661-1665.
7. Günther, Michael, Otto Müller, and Reinhard Blickhan. "Watching quiet human stance to shake off its straitjacket." *Archive of Applied Mechanics* 81.3 (2011): 283-302.
8. Günther, Michael, et al. "All leg joints contribute to quiet human stance: a mechanical analysis." *Journal of Biomechanics* 42.16 (2009): 2739-2746.
9. Günther, Michael, and Heiko Wagner. "Dynamics of quiet human stance: computer simulations of a triple inverted pendulum model." *Computer Methods in Biomechanics and Biomedical Engineering* 19.8 (2016): 819-834.
10. McLeish, R. D., and D. A. Arnold. "A foot-ground reaction force plate. Joint British Committee for Stress Analysis." *Proceedings of Conference on the Recording and Interpretation of Engineering Measurements*. 1972.

11. Croskey, Marguerite I., et al. "The height of the center of gravity in man." *American Journal of Physiology--Legacy Content* 61.1 (1922): 171-185.
12. Cheng, Kuangyou B. "Does knee motion contribute to feet-in-place balance recovery?" *Journal of Biomechanics* 49.9 (2016): 1873-1880.
13. Zehr, E. Paul, et al. "Neural regulation of rhythmic arm and leg movement is conserved across human locomotor tasks." *The Journal of Physiology* 582.1 (2007): 209-227.
14. Schmidt, M. W., et al. "Foot force direction in an isometric pushing task: prediction by kinematic and musculoskeletal models." *Experimental Brain Research* 150.2 (2003): 245-254.
15. Gruben, Kreg G., and Wendy L. Boehm. "Ankle torque control that shifts the center of pressure from heel to toe contributes non-zero sagittal plane angular momentum during human walking." *Journal of Biomechanics* 47.6 (2014): 1389-1394.
16. Banfi, Francesco, and Gabriele Ferrini. "Wavelet cross-correlation and phase analysis of a free cantilever subjected to band excitation." *Beilstein Journal of Nanotechnology* 3.1 (2012): 294-300.